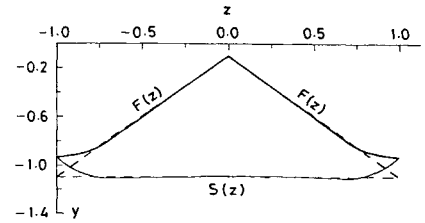

Fig. 1 Typical curved waverider (——) and a caret wing (- - -) and the supporting shock waves: $\gamma = 1.4$; $M_\infty = 10$; $\alpha = 25$ deg.; $b_0 = 0.1$; $b_2 = -2$

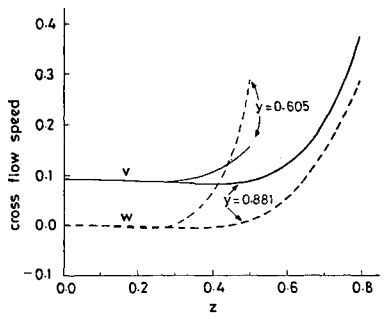

Fig. 2 Crossflow speeds for a curved waverider: $b_0 = 0.1$; $b_2 = -2$; $\gamma = 1.4$; $M_\infty = 10$; $\alpha = 25$ deg; $\Lambda = 45$ deg.

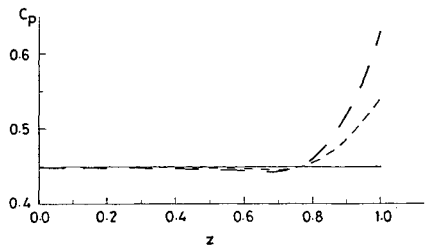

Fig. 3 Surface pressure of a caret wing and curved waveriders: $b_0 = 0.1$; $\gamma = 1.4$; $M_\infty = 10$; $\alpha = 25$ deg; $\Lambda = 45$ deg.; caret wing (——); $b_2 = -2$ (— —); $b_2 = -1$ (- - -).

TSLT and can be found by direct integration after introducing $\bar{z}$ into the pressure equations. It suffices here to give the final results as follows. First, for inverted V-shape wings, p is uniform and given by $p(y, z) = 2c_1 - 1 - c_2^2/\Omega^2$, where c_1 and c_2 are constants, and for a caret wing, it is also uniform and given by $p(y, z) = 1 + 2b_0$. The plane delta wing will have $p = 1 + 1/\Omega^2 - 1/\Omega^4[2 + 1/\Omega^2]$. The pressure has also been calculated in the cases where $F(z)$ is differentiable with $F(1) = 0$ and for curved waveriders, however, the details are omitted.

Results

Now we present some results. Figure 1 shows a caret wing and a curved waverider and their shock waves. The curved waverider shock wave has small (convex) curvature for all z. In Fig. 2, the crossflow speeds v and w on the lines $y = 0.605$ and 0.881 are shown. The figure shows that they remain almost uniform in the inboard of the flowfield but undergo some to considerable increase near the leading edges. Also noted is that the side wash w is almost zero (almost two-dimensional flow) in the inboard region. Figure 3 shows the surface pressure coefficient $C_p = (p_b - P_\infty)/\frac{1}{2}\rho_\infty U_\infty^2$, where p_b is the surface pressure and P_∞, ρ_∞, and U_∞, are the freestream pressure, density, and speed, respectively. Figure 3 shows the variation of C_p for a caret wing and two waveriders. The surface convex curvature, though small, has considerable effect on C_p near the leading edges.

References

[1]Messiter, A. F., "Lift of Slender Delta Wings According to Newtonian Theory," *AIAA Journal*, Vol. 1, No. 4, 1963, pp. 794–802.

[2]Hemdan, H. T., and Hui, W. H., "Unsteady and Steady Aerodynamic Forces of Slender Delta Wings According to Newtonian Theory," *Canadian Aeronautics and Space Journal*, Vol. 23, No. 4, 1976, pp. 238–251.

[3]Malmuth, N. D., "Three-Dimensional Perturbations on Hypersonic Wedge Flow," *AIAA Journal*, Vol. 2, No. 8, 1964, pp. 1383–1389.

[4]Hui, W. H., "Supersonic and Hypersonic Flow with Attached Shock Waves over Delta Wings," *Proceedings of the Royal Society of London, Series A*, Vol. 325, 1971, pp. 251–267.

[5]Hemdan, H. T., "Waverider Configurations According to Thin Shock-layer Theory," *Acta Astronautica*, Vol. 21, No. 8, 1990, pp. 571–582.

Direct Frequency Domain Calculation of Open Rotor Noise

Donald B. Hanson*
United Technologies Corporation,
Windsor Locks, Connecticut 06096

Introduction

TESTS of the Propeller Test Assessment (PTA) Aircraft[1] provided valuable near-field noise data on a large-scale (9-ft-diam) propfan operating at its 0.8 Mach number design condition. The nacelle was designed so that its tilt could be adjusted to three pitches for the evaluation of angular inflow effects. A recent paper[2] described a comparison of noise predictions from two frequency domain computer codes with data from the PTA experiment. Unsteady loading for input to the noise theory was computed using a time-accurate Euler method sensitive to angular inflow. One of the noise codes, identified as frequency domain, Hanson (FDH), was based on Hanson's near-field frequency domain theory.[3,4] It accounts for unsteady loading but not angular inflow. The other code, identified as frequency domain, Envia (FDE), was developed by Envia based on an unpublished theory that is sensitive to angular inflow. In Hanson's theory the tangential integration over the source volume is done analytically, leading to Bessel functions in the radiation formulas. From the description given in Ref. 2, it appears that Envia's method uses numerical integration over the tangential source coordinate. This numerical approach offers the advantage that propeller loading, geometry, and inflow angle can be represented more precisely for near-field calculations.

Theoretical waveforms and harmonic directivity patterns were compared in Ref. 2 with data from a series of microphones on a wing-mounted boom outboard of the propeller parallel to the propeller axis. Unfortunately, an error in the Envia code[5] invalidated the calculations in Ref. 2. However, predictions with the Hanson code appear to represent correct use of the axial inflow theory and are the motivation for this Note. In Fig. 1, the calculations are by Nallasamy et al. using the Hanson theory, and the data are boom microphone levels from Ref. 1 with corrections to the free field using the scattering theory of Ref. 6. (Starting with the forward microphone, the corrections were 0, 0.4, 0.7, 0.9, and 0.7 dB.) As shown in the figure, these calculations correlated well with data for two of the microphones aft of the plane of rotation but overpre-

Received Oct. 28, 1991; revision received Dec. 19, 1991; accepted for publication Dec 27, 1991.

*Principal Research Engineer, Propulsion Analysis Group, Mail Stop 1-3-BC52, Hamilton Standard Division, One Hamilton Road. Associate Fellow AIAA.

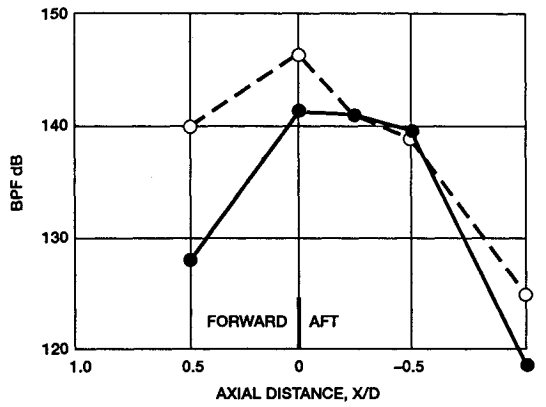

Fig. 1 Noise levels at constant sideline distance of 1.12 diameters for 1-deg nacelle downtilt at cruise condition: •, test data corrected to free field; ○, Hanson theory as reported by Nallasamy et al.[2]

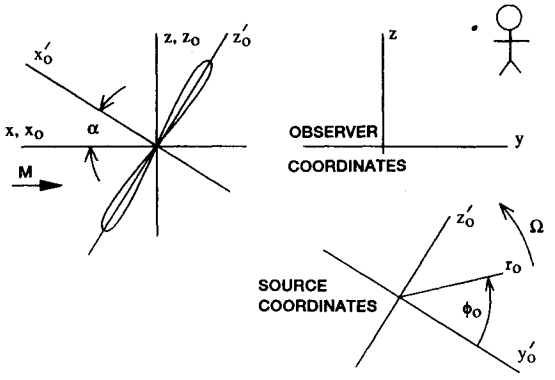

Fig. 2 Observer and source coordinates. Prop tilt is about the *y* axis.

dicted substantially at forward locations. The new theoretical formulation for propeller harmonic noise presented next is used to investigate the overprediction.

Like the early propeller theories[7] and those of Envia, the new formulation performs the circumferential integration numerically. However, unlike the early theories, sources are on the camber surface rather than on a disk, and the shaft can be tilted with respect to the inflow. The theory is evaluated by comparison with data and is then used to verify predictions from the earlier theory of Ref. 3, which did not include the shaft tilt effect. Predictions from the earlier theory tend to be supported by the new method and also by independent calculations reported by Farassat et al.[8]

Noise Theory

The basis of the following derivation is the same as for the theory developed by Hanson[9] for far-field noise of propellers with angular inflow. As shown in Fig. 2, the observer and propeller position are fixed with respect to the coordinates and the air flows uniformly from the left at Mach number M. Action of the blades is accounted for by replacing the blades with volume source terms representing the force that they impart to the air and their rate of volume displacement. The applicable linear wave equation for acoustic pressure is

$$\nabla^2 p - \frac{1}{c_0^2}\frac{\mathrm{D}^2 p}{\mathrm{D}t^2} = -\rho_0 \frac{\mathrm{D}q}{\mathrm{D}t} + \nabla \cdot \boldsymbol{F} \equiv -Q \tag{1}$$

where c_0 is the ambient speed of sound and the convective derivative, $\mathrm{D}/\mathrm{D}t = \partial/\partial t - V\partial/\partial x$, includes a minus sign because the fluid is moving in the negative x direction at speed $V = Mc_0$. The source term is Q in which ρ_0 is the ambient density, q is the volume displacement/unit time/unit volume, and $\boldsymbol{F}$ is the force on the fluid. For a propeller with B blades operating with its axis tilted as in Fig. 2, the disturbance at any fixed point in the coordinate system is periodic at radian frequency $B\Omega$. Thus, the source can be written as the Fourier series

$$Q = \sum_{m=-\infty}^{\infty} Q_m \exp(-imB\Omega t) \tag{2}$$

For an observer fixed with respect in the coordinates, the acoustic pressure has the same periodicity and can be written as $p = \Sigma\, P_m \exp(-imB\Omega t)$. Under these conditions, the solution to Eq. (1) is given by the Green's function integral

$$P_m(x) = \int G(x, x_0)\, Q_m(x_0)\, \mathrm{d}x_0 \tag{3}$$

with Green's function

$$G = \frac{e^{ik_m \sigma}}{4\pi S} \tag{4}$$

in which $k_m = mB\Omega/c_0$. With the definition $\beta^2 = 1 - M^2$,

$$S = \sqrt{X^2 + \beta^2(Y^2 + Z^2)}, \qquad \sigma = (MX + S)/\beta^2 \tag{5}$$

are called the amplitude radius and phase radius. These can be expressed in terms of the observer and source coordinates in Fig. 2 using the following:

$$\begin{aligned} X &= x - x_0 = x - (x_0' \cos\alpha - r_0 \sin\phi_0 \sin\alpha) \\ Y &= y - y_0 = y - r_0 \cos\phi_0 \\ Z &= z - z_0 = z - (x_0' \sin\alpha + r_0 \sin\phi_0 \cos\alpha) \end{aligned} \tag{6}$$

where, for the source, x_0, y_0, and z_0 are called flight coordinates because x_0 is aligned with the mean flow and, in the tilted system, r_0, ϕ_0, x_0' are called propeller coordinates.

The volume source Q must be expressed in terms of thickness and loading on the blade surfaces. This is done in propeller coordinates with reference to Fig. 3, which represents the cylindrical surface of constant r_0 unwrapped onto a plane. The curve $r_0\phi_c(r_0, x_0')$ is the intersection of the cylindrical surface with the camber surface of the reference blade. Force per unit volume $\boldsymbol{F}$ can be expressed in terms of the more physical force per unit area f as follows:

$$F(r_0, \phi_0, x_0', t) = f(r_0, x_0', t)\frac{1}{r_0}\delta(\phi_0 - \phi_c - \Omega t) \tag{7}$$

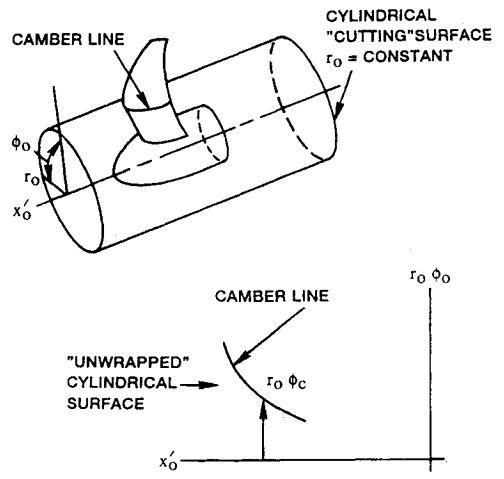

Fig. 3 Intersection of camber surface and cylindrical surface of radius r_0.

where the delta function places the force on the blade camber surface. Now, at any source position, the source only exists at time $t=(\phi_0-\phi_c)/\Omega$. Therefore, Eq. (7) may be replaced by

$$F(r_0,\phi_0,x_0',t)=\frac{1}{r_0}f[r_0,x_0',(\phi_0-\phi_c)/\Omega]\delta(\phi_0-\phi_c-\Omega t) \quad (8)$$

Replacing the delta function by its series representation transforms the source description from one discontinuous at the blade to a series of terms, each distributed continuously throughout the source volume:

$$F(r_0,\phi_0,x_0',t)=\frac{1}{2\pi r_0}f[r_0,x_0',(\phi_0-\phi_c)/\Omega]$$
$$\sum_{n=-\infty}^{\infty}\exp[in\,(\phi_0-\phi_c-\Omega t)] \quad (9)$$

For axial or angular inflow or for fixed flow distortion, each blade experiences identical loading history (shifted in time according to position in the hub) so that Eq. (9) can be made to represent loading on all B blades together:

$$F(r_0,\phi_0,x_0',t)=\frac{B}{2\pi r_0}f[r_0,x_0',(\phi_0-\phi_c)/\Omega]$$
$$\sum_{m-\infty}^{\infty}\exp\,[imB(\phi_0-\phi_c-\Omega t)] \quad (10)$$

Thus by comparison with Eqs. (1) and (2), the blade loading source for the mth harmonic is

$$F_m(r_0,\phi_0,x_0')=\frac{B}{2\pi r_0}f[r_0,x_0',(\phi_0-\phi_c)/\Omega]$$
$$\exp\,[imB\,(\phi_0-\phi_c)] \quad (11)$$

where f is just the waveform of loading on the reference blade, with time expressed in terms of azimuth angle ϕ_0.

A similar derivation applies to the thickness source. The volume displacement per unit time per unit volume can be expressed as

$$q(r_0,\phi_0,x_0',t)=U(r_0,\phi_0)h_{x'}(r_0,x_0')\frac{1}{r_0}\delta(\phi_0-\phi_c-\Omega t) \quad (12)$$

where h_x' is the derivative of the airfoil thickness distribution in the x_0' direction, and $U(r_0,\phi_0)$ is the blade section relative velocity, which varies with azimuth in the case of angular inflow. The same argument used earlier to account for multiple blades leads to

$$q_m(r_0,\phi_0,x_0')=\frac{B}{2\pi r_0}U(r_0,\phi_0)\;h_{x'}(r_0,x_0')\exp\,[imB(\phi_0-\phi_c)] \quad (13)$$

for the volume displacement source. The convective derivative acting on $q_m\exp(-imB\Omega t)$ gives

$$\left(\frac{Dq}{Dt}\right)_m=-imB\Omega q_m-V\frac{\partial q_m}{\partial x_0} \quad (14)$$

as needed for Eq. (3).

It is now straightforward to insert the sources, just derived, into the Green's function integral. If we write separate expressions for the thickness and loading noise harmonics with the notation $P_m=P_{Tm}+P_{Lm}$, the thickness component is

$$P_{Tm}=\rho_0\int\left(-imB\Omega q_m-V\frac{\partial q_m}{\partial x_0}\right)G\;dx_0 \quad (15)$$

Integration by parts is used to move the partial derivative from the source to the Green's function, and since we want to perform the source integration in the tilted propeller coordinates, we express the volume element dx_0 as $r_0\,d\phi_0\,dx_0'\,dr_0$. The final form becomes

$$P_{Tm}=\rho_0\int\int\int(-imB\Omega G+VG_x)q_m\;r_0\,d\phi_0\,dx_0'\,dr_0 \quad (16)$$

where G_x is $\partial G/\partial x_0$ and q_m was given in Eq. (13) The derivative of G is to be evaluated analytically in flight coordinates x_0, y_0, and z_0 using Eqs. (4-6) and then expressed in propeller coordinates r_0, ϕ_0, and x_0' for use in Eq. (16).

For the loading noise component, insertion of F_m into Eq. (3) gives

$$P_{Lm}=-\int\nabla\cdot F_m\;G\;dx_0=\int F_m\cdot\nabla G\;dx_0 \quad (17)$$

Here, we want to do the dot product in propeller coordinates because F_m is most easily expressed in this system. Hence,

$$P_{Lm}=\int\int\int F_m\cdot\nabla' G\;r_0\,d\phi_0\,dx_0'\,dr_0 \quad (18)$$

where $\nabla' G$ is the gradient in propeller coordinates. F_m can be evaluated either from the loading waveform using Eq. (11) or by reconstructing the loading waveform using loading harmonics. Equations (16) and (18) are convenient for direct computation because the Green's function derivatives can be done analytically and the sources can be represented in propeller coordinates. The volume integral requires a triple loop but, nevertheless, runs only a few seconds on a personal computer, or at least for the lower harmonics. Without further manipulation, the formulas account for angular inflow, all three components of the loading vector, and the unsteady thickness effect associated with variations in blade section relative velocity.

Comparison with Data

Predictions from the new theoretical formulation are compared here with data from Ref. 1 on the basis of directivity, spectrum, and waveform for the intermediate nacelle tilt. Then the trend with nacelle tilt is evaluated. Calculations that had been done some time ago at Hamilton Standard for structural analysis were used for unsteady blade loading input. These were based on quasisteady lifting line aerodynamics with distorted and angular inflow supplied by Lockheed from an airplane panel method.

The directivity comparison at blade passing frequency (BPF) is shown in Fig.4. Theory is reasonably accurate for the middle microphones as with the axial inflow theory. However, the forward microphone level is still substantially overpredicted. This reinforces the calculations of Ref. 2 but does not

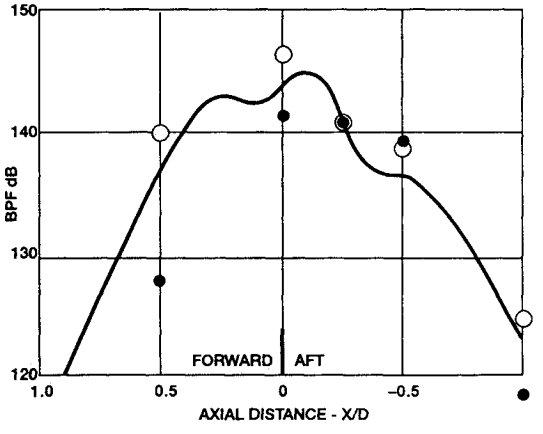

Fig. 4 Directivity along microphone boom at 1-deg downtilt: • and ○, same as Fig. 1; ———, present (free-field) theory.

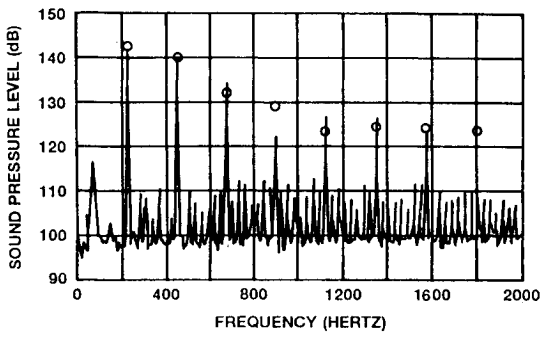

Fig. 5 Spectrum comparison at 0.25 diameter aft: ⊙, present theory corrected for amplification at boom.

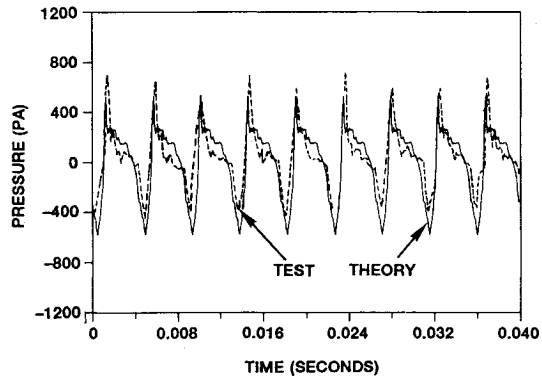

Fig. 6 Waveform comparisons for 1-deg downtilt at 0.25 diameter aft, not corrected for boom amplification.

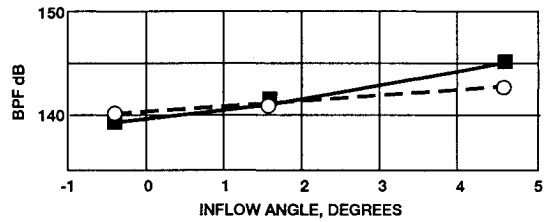

Fig. 7 Effect of nacelle tilt at 0.25 diameter aft: ■, data correct to free field; ○, present theory.

explain the discrepancy. Possible reasons include nonlinear propagation, reflection from the fuselage, and inadequate estimates of loading. Also, Farassat et al.[8] have noticed that measured noise directivity patterns on the fuselage suggest that the level of the forward microphone should be several dB higher. Since the agreement is good at the $0.25D$ aft position, the remaining figures address that microphone. Figure 5 shows that agreement with the upper harmonics at this location are excellent. (Here the boom corrections with Ref. 6 for the first four harmonics were 0.7, 3.1, 3.9, and 3.4 dB. The higher harmonics had to be estimated at 4.0 The waveform in Fig. 6 was generated using 15 harmonics. Agreement is good enough to indicate that the theory represents the physics properly. Finally, Fig. 7 shows trends with nacelle tilt at BPF. The new method predicts levels reasonably accurately, although the trend with tilt is weaker than that of the data.

Conclusions

A new theoretical method has been presented for prediction of harmonic noise of open rotors. By use of a numerical source integration, the method can account directly for effects such as shaft tilt, radial loading, unsteady volume displacement, and placement of the sources on the blade's actual camber surface. Fore and aft directivity predictions are moderately good, with deviations attributable possibly to nonlinear propagation or source effects and neglect of effects of testing on a real airplane such as reflections from the aircraft. It is hoped that further studies in progress with the new method will shed light on these issues.

References

[1]Bartel, H. W., and Swift, G., "Near-Field Acoustic Characteristics of a Single-Rotor Propfan," AIAA Paper 89-1055, April 1989.

[2]Nallasamy, M., Envia, E., Clark, B. J., and Groeneweg, J. F., "Near-Field Noise of a Single Rotation Propfan at an Angle of Attack," AIAA Paper 90-3953, Oct. 1990.

[3]Hanson, D. B., "Near-Field Frequency-Domain Theory for Propeller Noise," *AIAA Journal*, Vol. 23, No. 4, 1985, pp. 499-504.

[4]Hanson, D. B., "Unified Aeroacoustic Analysis for High Speed Turboprop Aerodynamics and Noise," NASA CR-4329, March 1991.

[5]Envia, E., private communication, April 1991.

[6]Hanson, D. B., and Magliozzi, B., "Propagation of Propeller Tone Noise Through a Fuselage Boundary Layer," *Journal of Aircraft*, Vol. 22, No. 1, 1985, pp. 63-70.

[7]Garrick, I. E., and Watkins, C. E., "A Theoretical Study of the Effect of Forward Speed on the Free-Space Sound-Pressure Field Around Propellers," NACA Rept. 1198, 1953.

[8]Farassat, F., Dunn, M. H., and Spence, P. L., "Advanced Propeller Noise Prediction in the Time Domain," *AIAA Journal*, Vol. 30, No. 9, 1992, pp. 2337-2340.

[9]Hanson, D. B., "Noise Radiation of Propeller Loading Sources with Angular Inflow," AIAA Paper 90-3995, Oct. 1990.

Advanced Propeller Noise Prediction in the Time Domain

F. Farassat*
NASA Langley Research Center, Hampton, Virginia 23665
and
M. H. Dunn† and P. L. Spence‡
Lockheed Engineering & Sciences Company, Hampton, Virginia 23666

Introduction

In a recent paper,[1] results from two frequency domain methods for predicting high-speed propeller noise by Hanson[2,3] and Envia (unpublished) were presented together with comparison with measured data. One of the objectives of the paper was to study the nonaxial inflow effect. The calculations by Hanson's method were performed using a computer code identified as frequency domain, Hanson (FDH) that does not account for nonaxial inflow effects. The acoustic code based on Envia's theory, identified as frequency domain, Envia (FDE), includes these effects. In Ref. 1, the measured acoustic data used for comparison with predictions were supplied by the Propeller Test Assessment (PTA) aircraft. This aircraft has a 2.74 m (9 ft) diameter, eight-bladed advanced propeller

Received Oct. 28, 1991; revision received Dec. 10, 1991; accepted for publication Dec. 27, 1991.

*Senior Research Scientist, Applied Acoustics Branch. Associate Fellow AIAA.

†Principal Engineer, Acoustics and Dynamics Department, 144 Research Drive. Member AIAA.

‡Senior Engineer, Acoustics and Dynamics Department, 144 Research Drive. Member AIAA.